Spatially varying super-lattice structures and linear fringes on graphite surface

2008 J. Phys.: Condens. Matter 20 225008

(http://iopscience.iop.org/0953-8984/20/22/225008)

J. Phys.: Condens. Matter **20** (2008) 225008 (6pp) doi:10.1088/0953-8984/20/22/225008

Spatially varying super-lattice structures and linear fringes on graphite surface

Shyam Kumar Choudhary and Anjan Kumar Gupta

Department of Physics, Indian Institute of Technology Kanpur, Kanpur 208016, India

Received 9 October 2007, in final form 5 March 2008
Published 25 April 2008
Online at stacks.iop.org/JPhysCM/20/225008

Abstract

We report on the scanning tunneling microscope (STM) observation of linear fringes and spatially varying super-lattice structure on (0001) graphite (HOPG) surface. The super-lattice structure, present in a region of a layer bounded by two straight carbon fibers, varies from a hexagonal lattice of 6 nm periodicity to nearly a square lattice of 13 nm periodicity. It then changes into a one-dimensional (1D) fringe-like pattern before relaxing into a pattern-free region. We attribute this surface structure to a shear strain giving rise to a spatially varying rotation of the affected graphite layer relative to the bulk substrate. Using this idea we can reproduce the spatially varying 2D lattice as well as the 1D fringes by simulation. The 1D fringes are found to result from a particular spatial dependence of the rotation angle.

1. Introduction

Since the discovery of the scanning tunneling microscope (STM) by Binnig and Rohrer [1], highly oriented pyrolytic graphite (HOPG) has been one of the most commonly used model surfaces for investigating and modeling of the STM imaging process. HOPG has a hexagonal structure with weakly coupled layers of graphene stacked in an ABAB . . . sequence. Graphene is a semi-metal with zero density of states (DOS) at E_F but a weak inter-layer interaction in graphite makes this DOS finite but small. This small DOS is quite sensitive to defects that influence the overlap of orbitals between layers [2]. This makes such defects easily visible by STM. Further, the weak inter-layer interaction makes such defects possible near the surface of HOPG. A widespread study of this material has led to the discovery of several types of crystal imperfections native to the basal plane of HOPG. These include stacking faults, graphite strands and fibers, broken or flaked layers [3], super-lattices [4–7] with periodicity of about ten nanometers or even larger, and the buckling of the top layer [8, 9].

Super-lattice structures in HOPG can occur due to disorientation of one or more of the graphite layers near the surface [5–7]. This type of super-lattice structure is commonly known as a moiré pattern and it arises as an interference pattern of two identical but slightly rotated periodic lattices. As first suggested by Kuwabara *et al* [5], this rotation by a small angle θ gives rise to a super-lattice of the same symmetry but with much larger lattice constant given by $D = d/(2\sin(\theta/2))$, with d the lattice constant of the original lattice. This super-lattice is rotated with respect to the original lattice by an angle $\phi = 30^\circ - \theta/2$.

In this paper we present an STM study of a spatially varying 2D super-lattice pattern and 1D fringes observed on HOPG(0001) surface near some defects. Such 2D patterns have been reported earlier by several groups and are widely believed to be due to the moiré interference [4–7]. Spatially varying periodicity patterns have also been reported before and have been attributed to a shear strain [10] or quantum confinement in a linear potential [11]. The electron coherence length required for such large scale quantum effects is of 1 μm order, which is impossible to have at room temperature in graphite [12]. The pattern observed here seems to be a result of an in-plane shear strain causing a spatially varying moiré rotation of a top layer. However, observation of linear fringes connected with a moiré pattern is a new finding. We also discuss how these fringes can arise from a shear strain using a simple theory similar to the one proposed by Amidror and Hersch [13, 14] for moiré patterns in optics. This approach gives us a better insight into the large scale structure of such patterns. An earlier model for moiré patterns in graphite is purely computational, based on the variation in local density of atoms [15]. In our model, the moiré patterns are examined in Fourier transformed k-space to quantify the variation in local stacking for a fixed as well as a spatially varying moiré rotation angle. Using this idea we can understand and simulate the above observed pattern and, in particular, the 1D fringes.

2. Experimental details

Experiments were done with a home built STM similar to the one described elsewhere [16]. This STM uses commercial

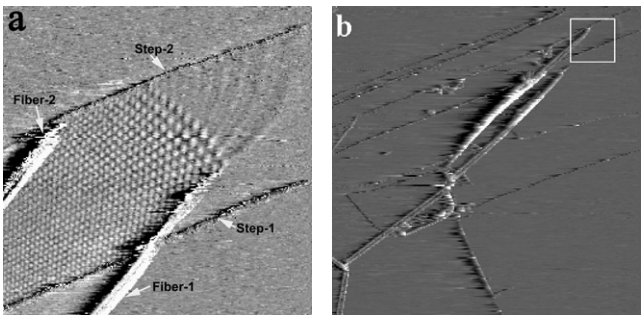

Figure 1. (a) STM image (0.32×0.32 μm^2 at 0.5 V and 0.2 nA) of HOPG showing a spatially varying super-lattice structure confined between fiber-1 and fiber-2 on the layers defined by step-1 and step-2. Near the termination of superstructure a 1D fringe pattern appears. (b) A later STM image (2.16×2.16 μm^2 at 0.8 V and 0.2 nA) showing a larger portion of fiber-1 and fiber-2. The area of the left image marked by the white square.

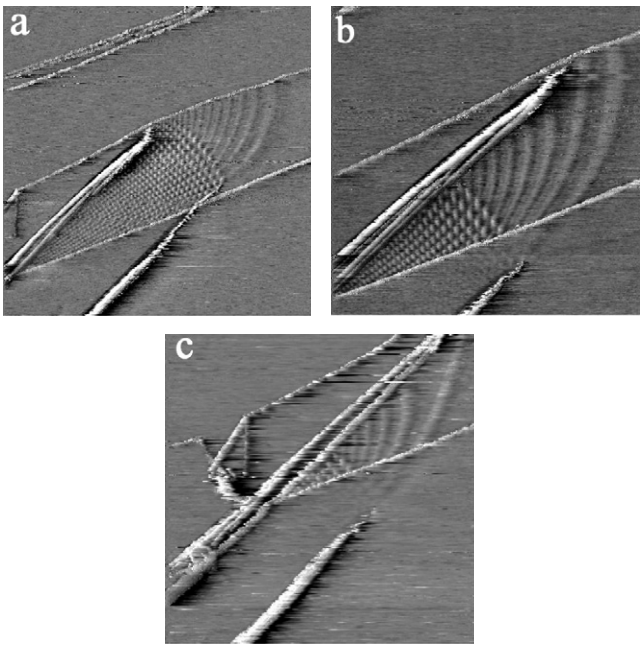

Figure 2. The topographic images of the super-lattice structure showing its evolution with the motion of fiber-1. (a) 0.52×0.52 μm^2, (b) 0.35×0.35 μm^2, (c) 0.43×0.43 μm^2 taken at 0.5 V and 0.2 nA.

electronics and software[1]. The data reported here were taken in ambient conditions. HOPG was fixed on the sample holder with a conducting epoxy and the sample was freshly cleaved using an adhesive tape before mounting it on the STM. Fresh cut $Pt_{0.8}Ir_{0.2}$ wire of 0.25 mm diameter was used as the STM tip. The images have been obtained in constant current (feedback on) mode. The images shown here are filtered to remove steps and spikes; however, for quantitative analysis we have used the unfiltered data.

3. Results

3.1. Spatially varying lattice and 1D fringes

Figure 1(a) shows a topographic image of a (0001) basal plane of HOPG with the super-lattice structure together with two steps and two carbon fibers. We mark these as fiber-1 and fiber-2 and step-1 and step-2. Step-1 is a double-layer step with a height of 0.7 ± 0.1 nm while step-2 is a single-layer step. These two steps divide the area into three terraces with the middle one having a super-lattice pattern confined between the two fibers as seen in the same figure.

Carbon fibers have been observed earlier by various groups on the graphite surface [4]. These, we believe, are long and thin ribbons or rolls of graphite created, presumably, during the cleaving process. The exact vertical location of the fibers relative to various visible layers is not so clear in this image. However, since the fibers are strictly limiting the pattern on the monolayer terrace defined by step-1 and step-2, we believe that these fibers are in contact with this affected layer. They may be either below or above this particular layer. If a layer is above the fiber it would go over the fiber with some buckling.

A relatively large area image including the patterned region is shown in figure 1(b). This image was taken later when the fiber-1 was fully relaxed as discussed in detail later. The region of the left image is marked by a square in the right one. The other ends of the two fibers are also visible in figure 1(b).

[1] RHK Technology, Troy, MI, USA.

Here we see that fiber-2 looks brighter below step-1 and fiber-1 has similar behavior but this is seen in figure 1(a). Here, both the fibers look less bright when they emerge from the covered layer(s) near the center of the image in figure 1(b).

As shown in figure 1(a) the super-lattice contains two regions, namely a 2D lattice extending to the end of fiber-1 and a 1D wave-like pattern starting from the fiber-1 end. The 1D fringes bend towards step-2 and terminate at this step. The 2D lattice continues beyond the fiber-2 end but terminates at step-2 in this image. The 1D pattern contains the same number of maxima and minima as the terminating 2D lattice. The 2D lattice is not uniform as it evolves from a hexagonal lattice deep inside the fibers to nearly a square lattice with much larger periodicity.

3.2. Pattern variation with fiber-1 motion

As we image this area repeatedly, fiber-1 becomes shorter in length as the whole fiber seems to recede. This may be due to some stress on the fiber. Several groups have reported various surface modifications in the STM experiments but the exact mechanism behind such modifications is not quite understood. We show three of the latter images in figure 2, depicting the pattern changing with fiber-1 withdrawal. The withdrawal of this fiber is not uniform with time as sometimes a significant length disappears in one scan and at other times it recedes gradually. Eventually the receding stopped and the length of the fiber stayed the same over a couple of days. One remarkable observation is the pinning of the boundary between the 2D super-lattice and the 1D fringes to the fiber-1 end. With the receding of fiber-1, the 1D fringes terminate on fiber-2 as opposed to step-2 as in earlier images. Moreover,

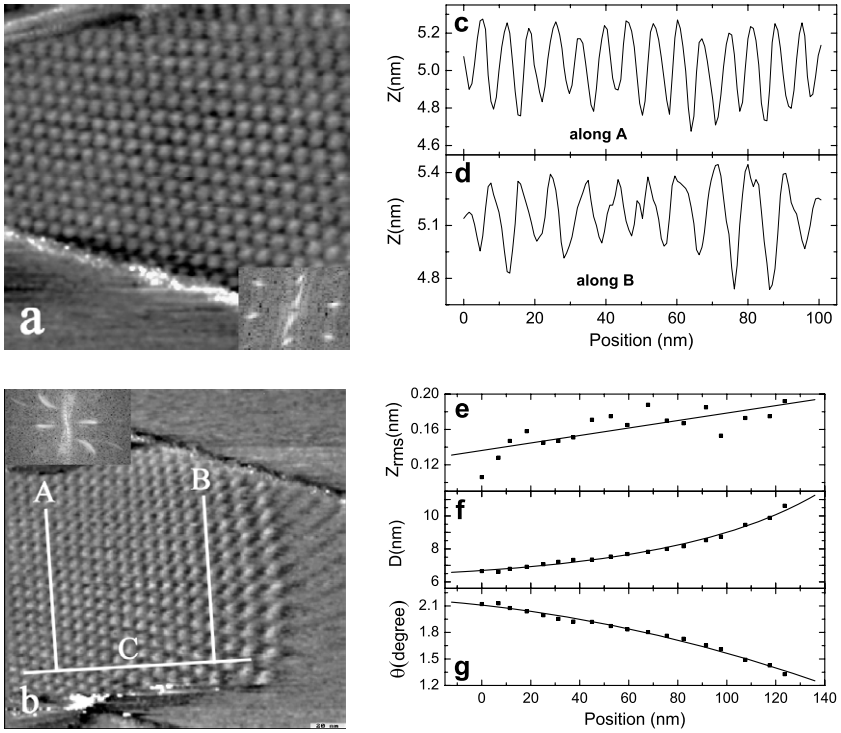

Figure 3. (a) Super-lattice pattern image (120 × 120 nm^2 at 0.5 V and 0.2 nA) taken deep inside the fibers, and (b) image (196 × 196 nm^2, 0.5 V/0.2 nA) taken near the boundary of the pattern. The insets show the respective Fourier transforms. (c) and (d) show the line scans along the lines A and B. (e), (f) and (g) show the variations (along line C) in rms corrugation, periodicity, and rotation, respectively.

the spatial extent and corrugation amplitude of 1D fringes increases together with some modifications in the large scale structure of the 1D pattern.

4. Analysis

Two close-up images of this pattern are shown in figure 3 in two different regions of the structure at different orientations of the image window as compared to the previous ones. These images have been taken at an early stage when fiber-1 was extending the most. As is apparent from the image shown in figure 3(a), the pattern deep inside the fibers (towards the left) is a hexagonal lattice of fixed periodicity. As we move out, the periodicity increases with the pattern evolving to an oblique lattice and then to nearly a square lattice as seen in figure 3(b). Fourier transforms (FT) of these images as shown in the inset also illustrate this variation. In detail, the FT in figure 3(a) shows six sharp spots while the FT in figure 3(b) has these spots elongated.

To analyze the periodicity variation carefully, line cuts were taken along various lines perpendicular to the line 'C' in figure 3(b). Two such representative lines are A and B along which the topographic height is plotted in figures 3(c) and (d). These lines were carefully chosen to pass over the bright spots of the 2D lattice. The periodicity along the lines perpendicular to C was found to be visibly constant but as one moves out along C this periodicity increases. The corrugation along the line C also varies. The RMS corrugation and periodicity as measured by line cuts perpendicular to C are plotted in figures 3(e) and (f) as a function of distance along the line C. The periodicity along such lines has been found from the average separation between peaks.

If we use the moiré rotation hypothesis, the rotation angle θ (between the top layer and the layers underneath) should also change spatially to get a varying lattice spacing D. Using $D = d/(2\sin(\theta/2))$ ($d = 0.246$ nm), we plot the variation of θ in figure 3(g). This varying θ implies that this rotated layer undergoes a shear as we move out of the fibers. The portion of this layer that is well inside the fibers has a constant rotation and the portion far outside the fibers is free of any moiré pattern and thus θ is zero. The intermediate region is strained with a changing θ and periodicity. As estimated from the periodicity, the angle θ changes from 2.3° to 1.3°. The 1D fringe pattern which has a close correlation with the 2D moiré pattern prompts us towards a common origin for the two patterns. We believe that the particular spatial dependence of θ is responsible for the 1D fringes as discussed later.

A second-order polynomial fit (as shown in figure 3(g)) for this θ variation gives an expression

$$\theta = A_0 - A_1 x - A_2 x^2 \qquad (1)$$

with $A_0 = (2.11 \pm 0.02)$ deg, $A_1 = (3.0 \pm 0.6) \times 10^{-3}$ deg nm^{-1}, $A_2 = (2.4 \pm 0.5) \times 10^{-5}$ deg nm^{-2}. This is also the expression for local angular orientation for a cantilever with one end clamped and the other end loaded[2]. By the

[2] Simple elasticity theory for a cantilever gives $\tan(\theta) = \frac{dy}{dx} = \frac{6F}{Ybd^3}(L^2 - x^2) \approx \theta$ (for small θ) with F as the force acting at one end of the cantilever, y as the vertical deflection at a given x. Y, L, d, and b are the Young's modulus, length, thickness, and the width of the cantilever, respectively.

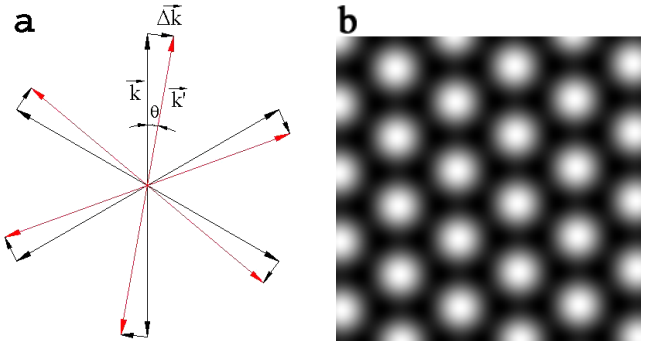

Figure 4. (a) The lattice vectors of the fixed (**k**) and slightly rotated (**k**′) hexagonal lattices and their differences (Δ**k**). In this figure the y-axis is pointing vertically up and x is pointing to the right. (b) Moiré interference pattern calculated using equation (2) with $\theta = 2.5°$. The size of the image is 25×25 nm^2.

(This figure is in colour only in the electronic version)

definition of strain, the maximum strain at a given x would be $\frac{d}{2}\frac{\mathrm{d}\theta}{\mathrm{d}x}$. To estimate the maximum strain, the $\frac{\mathrm{d}\theta}{\mathrm{d}x}$ is maximum at the boundary of the 2D super-lattice and 1D fringes and it is found from the polynomial fit (equation (1)) to be $(1.6 \pm 0.3) \times 10^{-4}$ rad nm^{-1}. At this location the thickness (d) is 115 nm. This point gives the largest stress, $\sigma_{\max} = 1.1 \pm 0.2$ GPa, using $Y = 121.9$ GPa [17] for graphite. For comparison, the macroscopic indentation experiments indicate that stress on the order of ≈1 GPa damages the surface of graphite [18]. On the other hand, Snyder *et al* [17] have shown that the stress required to induce dislocation motion on the basal plane of HOPG is of order 5–200 MPa.

5. Understanding the linear fringes from spatially varying moiré rotation

Here we describe a simple model to help understand and for simulating the large scale structure of the spatially varying moiré patterns. In 1D if we superimpose two 1D periodic patterns given by $\cos k_1 x$ and $\cos k_2 x$ ($|k_1 - k_2| \ll k_1, k_2$), we would see an interference pattern with periodicity $2\pi/|k_1 - k_2|$ in the superposed pattern (i.e., $\cos k_1 x \cos k_2 x$). In 2D if we superimpose two hexagonal patterns of slightly different reciprocal lattice vectors $\mathbf{k_i}$ and $\mathbf{k_i'}$ ($i = 1$–6), the resulting pattern in real space would come from the difference of the two sets of lattice vectors, i.e., ($\mathbf{k_i'} - \mathbf{k_j}$). The longest period variations would arise from $\Delta\mathbf{k_i} = \mathbf{k_i'} - \mathbf{k_i}$ (see figure 4), which are actually responsible for the observed moiré patterns. In 2D, the pattern could arise due to differences in both the magnitude and direction of **k** and **k**′ [13] but in the present case the direction mismatch is playing the major role. $\Delta\mathbf{k_i}$ as seen from figure 4, has a magnitude of $2k \sin(\theta/2)$ and the smallest angle that it makes with one of the $\mathbf{k_i}$ is $30° - \theta/2$. This is consistent with the aforementioned periodicity and angle of the moiré super-lattice. Now the moiré pattern in real space can be generated by the inverse Fourier transformation (IFT) of these six $\Delta\mathbf{k_i}$ vectors. This IFT gives a pattern described by

$$I(x, y) = I_0 + I_1[\cos(f_1) + \cos(f_2) + \cos(f_3)], \quad (2)$$

where I_0 and I_1 are two constants and

$$f_n = 2k \sin(\theta/2)\{-y \sin((n-1)\pi/3 + \theta/2) + x \cos((n-1)\pi/3 + \theta/2)\}. \quad (3)$$

Here $n = 1$, 2 or 3 and $k = 4\pi/\sqrt{3}d$, with d (= 0.246 nm) the real space ab-plane lattice parameter of graphite. Each cosine term in equation (2) gives rise to a 1D periodic pattern with bright and dark fringes along parallel straight lines (for constant θ). The bright fringes of $\cos f_n$ are described by the contours $f_n(x, y) = 2N\pi$, with N an integer. For a constant θ, the fringes due to the three cosine terms make an angle $\pi/3$ with each other and the sum of these three cosines leads to a 2D triangular lattice pattern. One such pattern is shown in figure 4(b) for $\theta = 2.5°$, $I_0 = 0$, and $I_1 = 1$. In this model, the $I(x, y)$ only quantifies the local stacking pattern.

This model can also be used for the geometrically transformed lattices [14], where the rotation angle is spatially varying. In this way we can model the spatially varying moiré patterns and understand their large scale structure. In particular, we can find an analytical condition on the spatial variation of the rotation angle that gives rise to the 1D fringes as follows. For spatially varying θ, the 1D fringes due to each $\cos f_n$ will have a spatially varying periodicity and, in general, these fringes may not be straight and parallel to each other. These fringes will be locally perpendicular to ∇f_n and their local periodicity can be quantified by $2\pi/|\nabla f_n|$. These f_n (see equation (3)) satisfy the condition

$$f_1 = f_2 - f_3. \quad (4)$$

For $I(x, y)$ to have a 1D pattern, the fringes due to the contributing cosine terms must be locally parallel to each other or, in other words, each f_n should have the same constant value contours. In particular, and as turns out to be the case for the observed 1D fringes, if the θ variation is such that $f_1 = C$ (a constant), then using equation (4), $f_2 = C + f_3$. For such θ variations $\cos f_1$ gives no fringes while the fringes due to $\cos f_2$ and $\cos f_3$ are locally parallel with the same local wavelength. Thus $I(x, y)$ would have only 1D fringes. A similar argument would also hold for $f_2 =$ constant or $f_3 =$ constant, which is obvious from symmetry considerations. The expression for f_1 (equation (3)) can be simplified to

$$f_1 = kx \sin\theta + ky(\cos\theta - 1), \quad (5)$$

and so for $f_1(x, y) = C$ we find

$$\theta(x, y) = \sin^{-1}\left[\frac{(C/k) + y}{\sqrt{x^2 + y^2}}\right] - \tan^{-1}\left(\frac{y}{x}\right). \quad (6)$$

In the small θ approximation we can neglect the $(\cos\theta - 1)$ term in comparison to the $\sin\theta$ term in equation (5) and this gives $\theta(x, y) = C/kx$. Here, one has to be careful in choosing the origin while using this form of $\theta(x, y)$. The same origin has to be used in calculating the $I(x, y)$ to ensure 1D fringes. In fact this choice of origin gives one more parameter in choosing $\theta(x, y)$.

A simulated pattern using the above ideas is shown in figure 5(b) together with the observed pattern in figure 5(a).

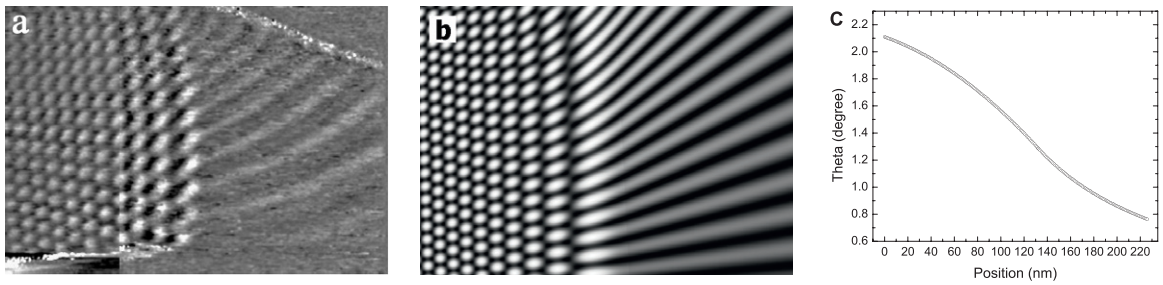

Figure 5. (a) STM image of the super-lattice pattern of varying periodicity and linear fringes (196 × 139 nm^2 at 0.5 V and 0.2 nA). The 2D pattern is present up to 100 nm and beyond this it changes into linear fringes. (b) Simulated image (see the text) of size 198 × 141 nm^2 with the θ variation shown in (c). In (b) the y-axis is pointing at an angle 3° to the upwards vertical and the x-axis is perpendicular to y and towards the right.

Here, we have used two different spatial forms of θ in different x intervals. We have used $\theta(x, y)$ as found in equation (1) for the 2D region, where θ changes from 2° to 1.29°. We use the small θ approximation for 1D fringes, i.e., $\theta(x, y) = C/k(x + a)$ for θ between 1.29° and 0.76°. The constants C/k and a are found to be 3.067 rad nm and 4.399 nm, respectively, by ensuring the continuity of θ and $\mathrm{d}\theta/\mathrm{d}x$ at $x = 132.3$ nm. This is necessary to keep the stress finite and continuous everywhere. For 1D fringes the required $\theta(x, y)$ is of the form of C/kx, so in figure 5, we have actually shown images of $I(x + a, y)$ with $a = 4.399$ nm. A plot of the θ variation used, as a function of x, is shown in figure 5(c). Since the 2D to 1D pattern boundary is pinned to the fiber-1 end we believe that there is a sudden change in spatial dependence of stress across this x causing a change in θ behavior that in turn is responsible for the boundary.

So far we have discussed a particular condition on θ for $f_1 = C$ that gives 1D fringes. The existence of 1D fringes requires that all the constant value contours of f_1, f_2, and f_3 are identical. One can find a more general condition on θ for getting 1D by considering f_1, a function of some scalar function $\phi(x, y)$. From figure 5(a) we see that the observed 1D fringes connect smoothly to the rows of bright spots coming from cos f_2 and cos f_3 while the rows of bright spots due to cos f_1 terminate before the 1D fringes. This means that cos f_1 is not contributing to the observed 1D fringes and cos f_1 has to be constant in this region. So $\theta = C/kx$ is the only possibility for the observed fringes in a small θ approximation.

6. Discussion

Our simulation nicely captures most of the details of the observed pattern except for the curvature of the 1D fringes. For the curvature in 1D fringes, we find that any modification in spatial dependence of θ from C/kx affects the 1D nature more seriously than producing the curvature. Incidentally, using the exact form of θ as in equation (6) as opposed to its approximate form for C/kx does not give the curvature either. Here, we believe that our approach of varying only the directions of the $\mathbf{k}'$ and not their magnitude is a bit oversimplified, though it captures the general structure of both the 1D and 2D patterns. However, to get both the direction and magnitude of $\mathbf{k}'$ requires a detailed understanding of the strain field in the affected region. This is not possible from the STM images alone, as we have to know the stresses on the boundaries to solve the complete boundary value problem using elasticity theory.

As pointed out earlier, we should be cautious in using this model as this does not describe the quantitative contrast of an STM image. For instance, this model cannot explain the variation in corrugation amplitude of the 2D super-lattice with its periodicity as seen from figure 3(e). The STM contrast here actually represents a DOS variation as our local tunneling spectra show that the bright regions are more metallic than the dark ones, consistently with earlier work by Kuwabara *et al* [5]. As of now, no calculations on electronic DOS on moiré patterns in graphite exist. A computational model was proposed by Hentschke *et al* [19] and reviewed by Pong *et al* [15] which is based on the variation in local density of atoms. In a sense our $I(x, y)$ also quantifies the local density of atoms but our model is more appropriate for the analytical understanding of the large scale structure of the spatially varying moiré patterns.

7. Conclusions

In conclusion, we have studied a spatially varying 2D and a connected 1D super-lattice structure on HOPG. This is the first observation of such 1D fringes connected to a 2D moiré lattice and we attribute this pattern to a spatially varying moiré rotation of a top graphite layer. The spatially varying rotation implies a shear strain in this layer. We have also described a simple model for understanding spatially varying moireé patterns. This model can successfully simulate the observed pattern by using a spatially varying rotation angle. The 1D fringes are found to arise from a particular spatial dependence of the moireé rotation angle.

Acknowledgments

Financial support from IITK under the 'Initiation Grant' scheme and from the MHRD of the Government of India is gratefully acknowledged. Partial funding from the DST of the Government of India is also acknowledged. S K Choudhary acknowledges financial support from the University Grant Commission, Government of India.

References

[1] Binnig G, Rohrer H, Gerber Ch and Weibel E 1982 *Phys. Rev. Lett.* **49** 57
[2] Kilic C, Mehrez H and Ciraci S 1998 *Phys. Rev.* B **58** 7872
[3] Chang H and Bard A J 1991 *Langmuir* **7** 1143
Clemmer C and Beebe T 1991 *Science* **251** 640
Snyder S, Foecke T, White H and Gerberich H 1992 *J. Mater. Res.* **7** 341
[4] Pong W-T and Durkan C 2005 *J. Phys. D: Appl. Phys.* **38** R329
[5] Kuwabara M, Clarke D R and Smith D A 1990 *Appl. Phys. Lett.* **56** 2396
[6] Rong Z Y and Kuiper P 1993 *Phys. Rev.* B **48** 17427
[7] Xhie J, Sattler K, Ge M and Venkateswaran N 1993 *Phys. Rev.* B **47** 15835
[8] Pong W T, Bendall J and Durkan C 2005 *Japan. J. Appl. Phys.* 1 **44** 5443
[9] Choudhary S K and Gupta A K 2007 *Japan. J. Appl. Phys.* 1 **46** 7450
[10] Bernhardt T M, Kaiser B and Rademann K 1998 *Surf. Sci.* **408** 86
[11] Harigaya K, Kobayashi Y, Takai K, Rvier J and Enoki T 2002 *J. Phys.: Condens. Matter* **14** L605
[12] Berger C, Song Z, Li X, Wu X, Brown N, Naud C, Mayou D, Li T, Hass J, Marchenkov A N, Conrad E H, First P N and de Heer W A 2006 *Science* **312** 1191
[13] Amidror I and Hersch R D 1996 *J. Opt. Soc. Am.* A **13** 974
[14] Amidror I and Hersch R D 1998 *J. Opt. Soc. Am.* A **15** 1100
[15] Pong W-T and Durkan C 2005 *Japan. J. Appl. Phys.* 1 **44** 5365
[16] Gupta A K and Ng K-W 2001 *Rev. Sci. Instrum.* **72** 3552
[17] Snyder S R, Gerberich W W and White H S 1993 *Phys. Rev.* B **47** 10823
[18] Skinner J, Gane N and Tabor D 1971 *Nat. Phys. Sci.* **232** 195
[19] Hentschke R, Schurmann B and Rabe J 1992 *J. Chem. Phys.* **96** 6213